OATAO

Open Archive Toulouse Archive Ouverte

Open Archive Toulouse Archive Ouverte

OATAO is an open access repository that collects the work of Toulouse researchers and makes it freely available over the web where possible

In situ injection of THF to trigger gas hydrate crystallization: Application to the evaluation of a kinetic hydrate promoter

Marvin Ricaurte, Jean-Philippe Torré, Joseph Diaz, Christophe Dicharry *

Univ. Pau & Pays Adour, CNRS, TOTAL – UMR 5150 – LFC-R – Laboratoire des Fluides Complexes et leurs Réservoirs, Avenue de l'Université, BP 1155 – PAU, F-64013, France

This paper investigates an original method to efficiently trigger gas hydrate crystallization. This method consists of an in situ injection of a small amount of THF into an aqueous phase in contact with a gas-hydrate-former phase at pressure and temperature conditions inside the hydrate metastable zone. In the presence of a CO_2–CH_4 gas mixture, our results show that the THF injection induces immediate crystallization of a first hydrate containing THF. This triggers the formation of the CO_2–CH_4 binary hydrate as proven by the pressure and temperature reached at equilibrium. This experimental method, which "cancels out" the stochasticity of the hydrate crystallization, was used to evaluate the effect of the anionic surfactant SDS at different concentrations, on the formation kinetics of the CO_2–CH_4 hydrate. The results are discussed and compared with those published in a recent article (Ricaurte et al., 2013), where THF was not injected but present in the aqueous phase from the beginning and at much higher concentrations.

1. Introduction

Gas hydrates are nonstoichiometric crystalline compounds formed of low molecular weight gas molecules enclathrated into a three-dimensional lattice framework of hydrogen-bonded water molecules (Sloan and Koh, 2008). They are currently attracting significant interest for potential practical applications such as refrigeration and air conditioning (Delahaye et al., 2011; Jerbi et al., 2010), seawater desalination (Park et al., 2011; Wang et al., 2013), energy storage and transportation (Rehder et al., 2012; Veluswamy and Linga, 2013), and capture of greenhouse gases (Ricaurte et al., 2013; Tang et al., 2013). One key issue for an economically viable application of any such hydrate-based process is the slow rate of hydrate formation. Kinetic hydrate promoters (KHP), chemical additives, which are generally surfactants (e.g. sodium dodecyl sulfate, SDS), can be used as a possible strategy for improving the hydrate formation kinetics (Gayet et al., 2005; Tang et al., 2013; Zhong and Rogers, 2000). Certain mixtures of KHP and thermodynamic hydrate promoters (e.g. mixtures of SDS and tetrahydrofuran (THF)) have also proven efficient in increasing the formation rate of hydrates formed with pure gases (e.g. CO_2 (Tang et al., 2013; Torré et al., 2011, 2012)) and gas mixtures (e.g. CO_2–CH_4 (Ricaurte et al., 2013)).

Direct observations of hydrate crystallization suggest that what forms at the water/gas (w/g) interface when additives are present is a porous hydrate structure, as opposed to the hydrate crust usually observed without additives (Gayet et al., 2005). In many cases, the porous hydrate structure is seen to spread up the reactor walls (above the level of the w/g interface) and to suck up the remaining water by capillarity. The high exchange area thus maintained between the gas and water phases fosters ongoing hydrate crystallization. Efficient kinetic additives therefore not only enhance the kinetics of hydrate formation but also often increase the amount of gas hydrate formed.

The performance of a KHP is often quantified by measuring the gas consumption rate at the anticipated pressure and temperature conditions for the target application. This is only feasible, however, if the point at which it is measured
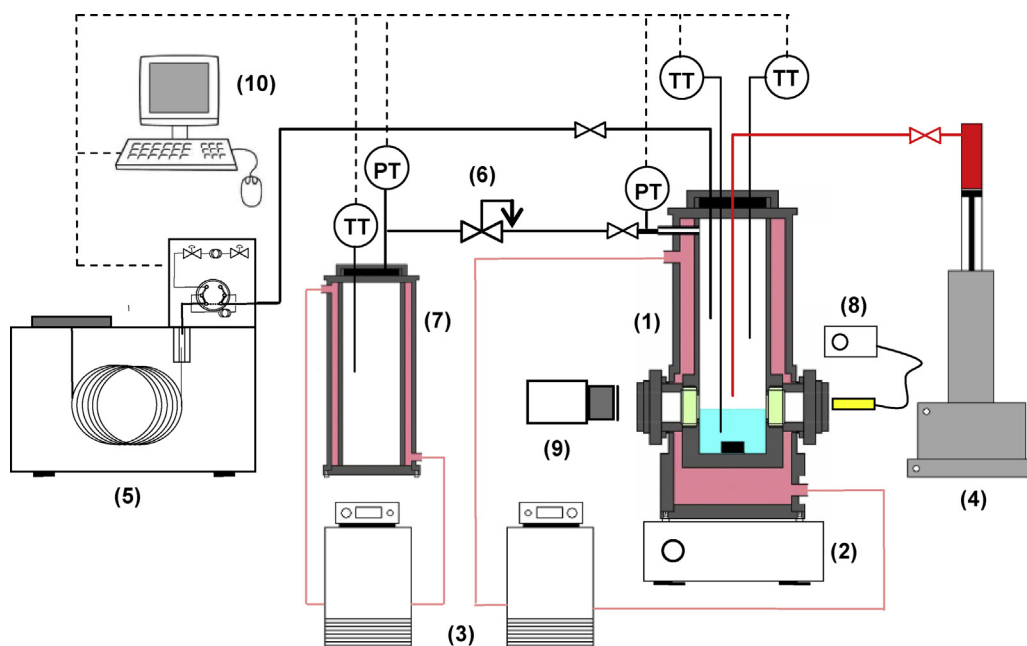

Fig. 1 – Schematic diagram of the experimental setup: (1) hydrate forming cell; (2) magnetic agitator; (3) thermostatic baths; (4) syringe pump; (5) high pressure gas chromatograph, (6) pressure reducing valve, (7) gas storage vessel; (8) lighting system; (9) video camera; and (10) data acquisition system.

lies inside the hydrate metastable zone (HMZ), i.e. where subcooling (the difference between the hydrate equilibrium temperature and the system temperature at the experimental pressure) is not too high. Outside this zone, hydrate will crystallize before reaching that point. Because the stochasticity of hydrate nucleation in the HMZ is generally very high, various authors have developed specific experimental protocols, based on the "water memory" effect, in an attempt to force the system to crystallize at the target point (Adeyemo et al., 2010; Dicharry et al., 2013; Duchateau et al., 2009, 2010; Okutani et al., 2008; Sefidroodi et al., 2013). These methods take advantage of the residual structures remaining in solution after a prior hydrate formation/decomposition cycle to reduce the stochastic character of hydrate crystallization in the subsequent formation cycle. The first major difficulty in implementing such protocols is that many preliminary experiments usually have to be run to determine the appropriate initial formation/decomposition conditions so that the subsequent hydrate crystallization can begin at the desired pressure and temperature. Next comes the difficulty, when the mutual solubility of the components present in the system is not negligible (e.g. the solubility of CO_2 in the water phase), of ensuring that hydrate crystallization will not occur until after the system has reached solubility equilibrium.

The main objective of the present work is to propose an experimental method for precisely controlling when hydrate crystallization will begin. The method consists of triggering hydrate crystallization by sudden injection of a small amount of a gas hydrate former (here THF) into the aqueous phase of the system under study, equilibrated at given pressure and temperature conditions inside the HMZ. In the first part of this article, we present the experimental setup and describe the protocol followed to trigger hydrate crystallization. The advantages of the method are illustrated by quantifying the effect of SDS used at different concentrations on the formation kinetics of the CO_2–CH_4 hydrate and comparing the results with those published in a recent paper (Ricaurte et al., 2013),

where THF was not injected but initially present (at a higher concentration) in the aqueous phase.

2. Experimental

2.1. Materials

The CO_2/CH_4 gas mixture, supplied by Air Liquide, contained 75.02 ± 0.50 mol% of CO_2 and 24.98 ± 0.50 mol% of CH_4. THF (purity > 99.9%) and SDS (purity > 98%) were supplied by Sigma–Aldrich and Chem. Lab., respectively. Ultra-pure water (resistivity of $18.2\,M\Omega$ cm) produced by a laboratory water-purification system from Purelab was used to prepare the SDS solutions.

2.2. Apparatus

The experimental setup used for hydrate formation is depicted schematically in Fig. 1. The hydrate-forming cell is a jacketed cylindrical vessel in titanium with an internal volume of $299.7 \pm 0.9\,cm^3$. It has two sapphire windows of diameter 20 mm, and a star-shaped magnetic agitator for stirring. A jacketed gas-storage vessel and a high-pressure syringe pump (ISCO 100 DM) are used respectively to load the CO_2/CH_4 gas mixture and inject the THF into the cell. A gas chromatograph (Agilent, Model GC6980), equipped with a high pressure sampling system, a capillary column (model *HP-PLOT-Q* from Agilent) and a thermal conductivity detector (TCD) is connected to the cell and used to sample and analyze the gas phase composition during the experiment. The gas and liquid temperatures in the cell are measured using PT100 probes with an accuracy of ± 0.2 K and the cell pressure is measured with a 0–10 MPa pressure transducer accurate to within ± 0.02 MPa. The data are recorded every second by a computer running an in-house LabView® program. Proceedings in the cell during the experiment are visualized via a CCD camera (*OptiaII from Creative Labs*).

2.3. Experimental procedures

The cell is loaded with $65.0 \pm 0.1\,cm^3$ of an aqueous solution containing SDS, then purged twice with the CO_2/CH_4 gas mixture to remove the remaining air in the system and pressurized with 4 MPa of the gas mixture, at 293 K (these pressure and temperature conditions are outside the hydrate stability zone). As illustrated in Fig. 1, the level of the SDS solution in the cell reaches the middle of the sapphire windows and the tip of the tubing used for THF injection is located in the gas phase a few mm above the w/g interface. The agitator is started and set to 600 rpm. The cell is cooled at a rate of 0.9 K/min to the target temperature $T_{targ} = 275\,K$, which is inside the HMZ (Ricaurte et al., 2013). One hour after the pressure reached a constant value at that temperature, the agitator is stopped (the hydrate formation experiment is thus conducted under quiescent conditions) and $0.30 \pm 0.01\,cm^3$ of THF is injected in one shot at the rate of $10\,cm^3$/min with the syringe pump. This quantity represents a THF concentration of 4000 ppm (by weight) in the aqueous phase. In the cell, temperature is maintained at T_{targ} until pressure stabilizes. Finally, the cell temperature is raised to 293 K again, at a rate of 1.5 K/min.

The experiments with THF initially present in the aqueous phase were conducted in the same cell, with the same volumes of aqueous and gas phases but with higher concentrations of THF (10,000–40,000 ppm). The protocol followed is as detailed in our previous work (Ricaurte et al., 2013), the main difference being that, here, the cell was pressurized at 4 MPa and
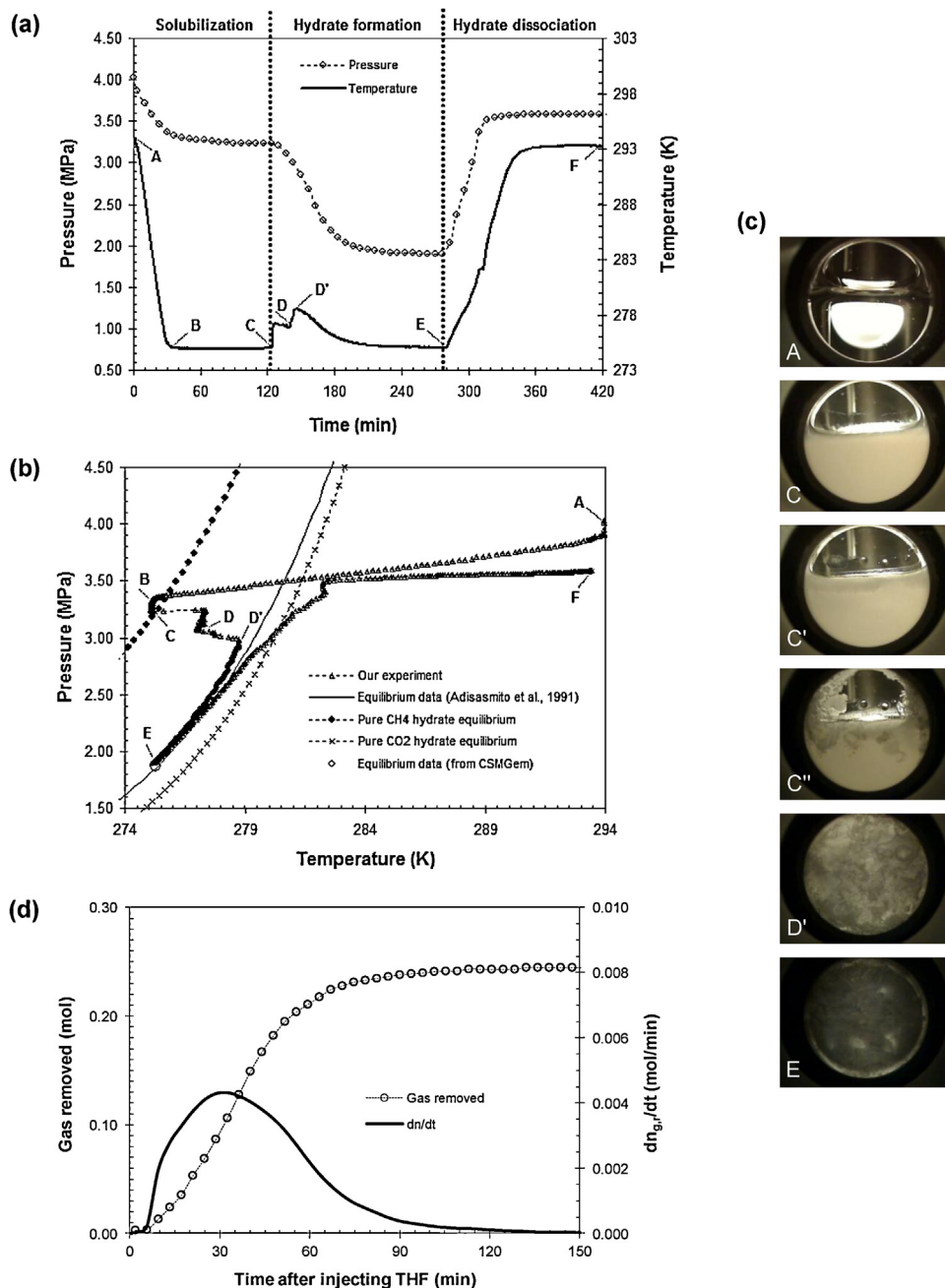

Fig. 2 – Typical curves obtained when injecting THF to trigger the hydrate crystallization: (a) cell pressure and cell temperature as a function of time; (b) pressure–temperature diagram, (c) set of snapshots (see the text for details) and (d) amount of gas removed from the gas phase and gas enclathration rate as a function of time. Conditions are: [SDS] = 3000 ppm, [THF]$_{injected}$ = 4000 ppm.

the aqueous phase was agitated at 293 K for 120 min to obtain gas solubilization before decreasing the cell temperature to T_{targ}.

3. Results and discussion

3.1. Triggering hydrate crystallization by injecting a small amount of THF into the aqueous phase

Fig. 2 shows the typical curves obtained when hydrate crystallization is triggered by the injection of 4000 ppm of THF into a SDS solution. Fig. 2(a) represents cell pressure and temperature as a function of time. From point A to B, the decrease in cell pressure is caused by both gas contraction and increase in gas solubility with temperature decrease. Pressure in the cell stabilizes at a constant value (here of about 3.2 MPa) less than 1 h after the temperature has reached T_{targ}. Point C is where THF was injected into the aqueous phase bringing, seconds later, a sharp rise in the cell temperature caused by the onset of the hydrate crystallization. This was followed by a second increase, a few minutes later (point D). The steep decrease in cell pressure observed after point D′ reflects the formation of a large quantity of hydrate. At point E, temperature and pressure in the cell attain constant values, indicating that the system has reached equilibrium. When the system is heated from point E to F, the increase in cell pressure is caused by gas expansion, decreased gas solubility and decomposition of the hydrate formed in the previous stage.

Fig. 2(b) shows the same experimental data as in Fig. 2(a) but plotted in a pressure–temperature diagram. For this experiment, it can be seen that the THF injection point (point C) is located deep inside the CO_2-hydrate stability zone, very close to the CH_4-hydrate equilibrium curve. The graph also clearly shows that the main gas consumption occurs from point D′, after the second peak in cell temperature observed in Fig. 2(a). The pressure reached by the system at the end of hydrate formation at T_{targ} (point E) almost perfectly matches both the equilibrium pressure of the CO_2–CH_4 binary hydrate given by the empirical correlation of Adisasmito et al. (1991) using the gas composition measured at point E, and that obtained using the CSMGem software program (Sloan and Koh, 2008).

The series of snapshots in Fig. 2(c) show the appearance of the system: (i) at the beginning of the experiment (snapshot A), (ii) during the THF injection (snapshot C), (iii) when hydrate crystallization starts (snapshot C′), and 1 min later (snapshot C″), (iv) when its rate is highest (snapshot D′), and (v) when it is finished (snapshot E). As will be noticed from snapshots C′ and C″, hydrate crystallization first occurs at the w/g interface (in the immediate vicinity of the THF injection zone) before expanding to the bulk liquid phase. It is in all probability triggered by local supersaturation of the gas hydrate
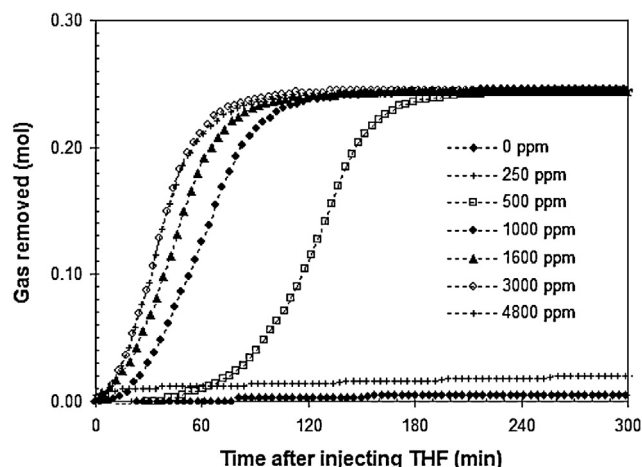

Fig. 3 – Amount of gas removed from the gas phase as a function of time. Conditions are: [SDS] = 0–4800 ppm, [THF]$_{injected}$ = 4000 ppm.

former THF near its injection point. This assumption is supported by the fact that, in a further experiment where pure water was injected into a 3000 ppm SDS solution instead of THF, no hydrate formation was observed.

Some of the hydrate particles formed is observed to climb up the wall of the cell, and a few minutes after the sapphire windows have been totally covered up, many dark efflorescence appear and rapidly spread across the solid phase (snapshot D′). Their formation is always concomitant with a sharp increase in the gas consumption rate.

The mechanisms of hydrate formation put forward in our previous study (Ricaurte et al., 2013) – which was performed on the same system except that THF was not injected but present in the aqueous phase from the start, and at a concentration 10 times higher than here – seem to occur in the present case too. On the one hand, the presence (or injection) of THF leads to the formation of a mixed hydrate containing THF, CO_2 and CH_4, which then act as seeds for the formation of the CO_2–CH_4 binary hydrate. On the other hand, the DS^- anions, which are present in the aqueous solution, adsorb on the hydrate particles (Zhang et al., 2008) and prevent them from agglomerating into large compact masses. The water not converted to hydrate is absorbed into the porous hydrate structure formed, thus – maintaining a high exchange area between the water and gas phases, which is conducive to enhanced formation kinetics and to achieving a high water-to-hydrate conversion (Torré et al., 2012).

Fig. 2(d) shows the mole number of gas removed from the gas phase (or enclathrated in the hydrate phase), $n_{g,r}$ and the gas enclathration rate, $dn_{g,r}/dt$ as a function of time, with $t = 0$ min corresponding to the THF injection point.

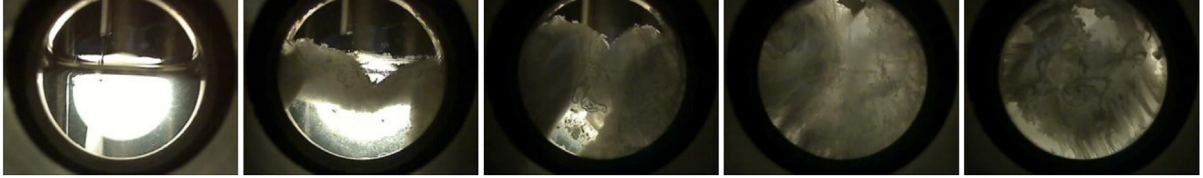| Table 1 – Values of the maximum enclathration rate, $(dn_{g,r}/dt)_{max}$ as a function of SDS concentration.							
	[THF] (ppm)	[SDS] (ppm)					
		0	250	500	1000	1600	3000	4800
$(dn_{g,r}/dt)_{max} \times 10^3$ (mol/min)	4000[a]	~0	~0	2.8	3.3	3.8	4.5	4.5
	40,000[b]	~0	ND	4.6	5.6	6.5	6.6	6.2

ND, not determined.
[a] THF is injected into the aqueous phase.
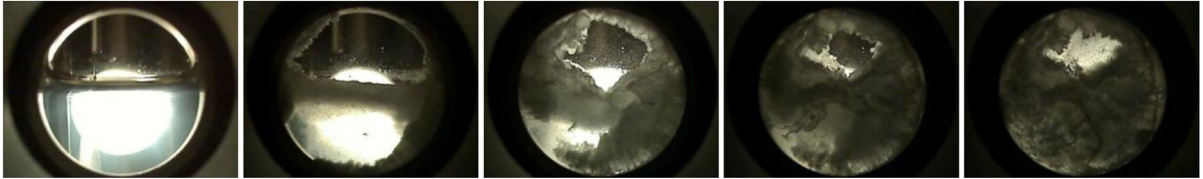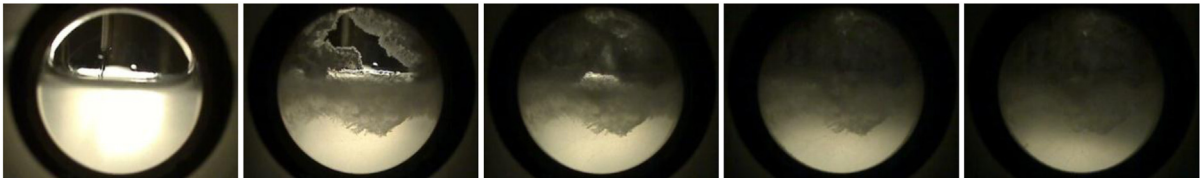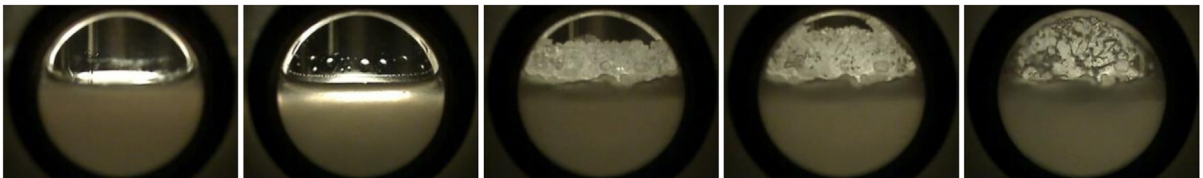[b] THF is initially present in the aqueous phase.
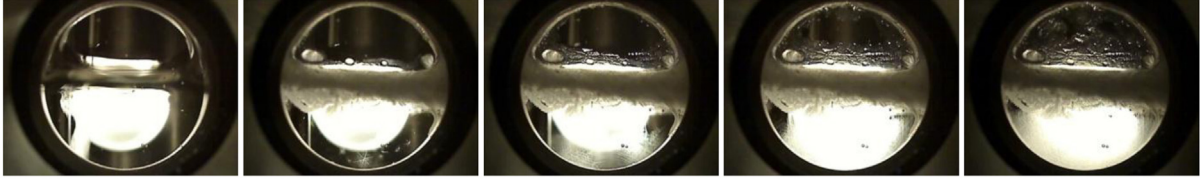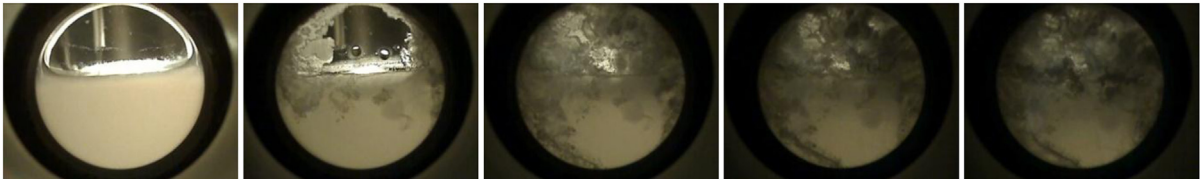
Fig. 4 – Snapshots of each system taken at t = 0, 1, 2, 3 and 5 min after injecting THF. [SDS] = 0–4800 ppm, [THF]$_{injected}$ = 4000 ppm.

$n_{g,r}$ is calculated using Eq. (1):

$$n_{g,r} = \sum_i n_{g,r}^i \tag{1}$$

with

$$n_{g,r}^i = n_g^i|_{t_{init}} - n_g^i|_{t_{init}} = \frac{y^i PV}{zRT}\Big|_{t_{init}} - \frac{y^i PV}{zRT}\Big|_{t_{final}} \tag{2}$$

where the superscript i corresponds to the gas (CO_2 or CH_4) present in the gas mixture, y^i is the molar concentration of i in the gas mixture, z the compressibility factor calculated using the Peng–Robinson Equation of State, P the cell pressure, T the cell temperature, V the gas phase volume, and t_{init} and t_{final} the initial and final times of the experiment.

The gas begins to be consumed by the hydrate phase almost immediately after the THF injection. $dn_{g,r}/dt$ peaks about 30 min after the THF injection, and

then decreases to almost zero about 100 min after the peak.

It is worth noting that the same behavior was observed on injecting 400 ppm of THF (i.e. $0.03\,\mathrm{cm^3}$ of THF) instead of 4000 ppm, but because of the difficulty of accurately injecting such a small amount of THF, we decided to use 4000 ppm in all the experiments presented in the rest of this work.

3.2. Application of the "hydrate triggering method" for studying the effect of SDS on the crystallization kinetics of the CO_2–CH_4 hydrate

The formation kinetics of the CO_2–CH_4 hydrate was quantified for different concentrations of SDS using the same material and protocol as described in Section 2. Fig. 3 shows $n_{g,r}$ as a function of time for the different SDS concentrations used. For each curve, the time $t=0$ min corresponds to the THF injection point. Snapshots taken of each system during the initial 5 min following the THF injection are provided in Fig. 4. The maximum values of the gas enclathration rate, $(dn_{g,r}/dt)_{max}$ obtained for the different SDS concentrations are reported in Table 1.

Although the THF injection triggered hydrate crystallization in all the cases investigated, substantial differences in the crystallization behavior were observed depending on the SDS concentration used. In the absence of SDS, a hydrate crust rapidly formed at the w/g interface (snapshots (a) in Fig. 4), preventing the water phase located below it from being converted to hydrate. The total amount of gas removed from the gas phase $(n_{g,r})_{max}$ and $(dn_{g,r}/dt)_{max}$ were therefore almost zero in this case. For the system with 250 ppm of SDS, the hydrate layer formed at the w/g interface was thicker than without SDS, and progressively covered the sapphire windows (snapshots (b) in Fig. 4); $(n_{g,r})_{max}$ and $(dn_{g,r}/dt)_{max}$ remained, however, very small. For SDS concentrations of 500 ppm and higher, both $(n_{g,r})_{max}$ and $(dn_{g,r}/dt)_{max}$ drastically increased. Although the gases were enclathrated at a much slower rate for the system with 500 ppm of SDS than for higher concentrations, the same total amount of gas was removed from the gas phase for all these concentrations (Fig. 3). For the SDS concentration of 4800 ppm, the onset of hydrate crystallization appeared to be delayed for more than 1 min compared to the other systems (not detectable on the plot in Fig. 3 but clearly visible between the two first snapshots of each set in Fig. 4). The quantity $(dn_{g,r}/dt)_{max}$ however, reached the same value as for the system with 3000 ppm SDS (Table 1).

Note that Ricaurte et al. (2013) reported the same trends for the systems with 40,000 ppm of THF in the aqueous phase, namely, no significant amount of gas removed from the gas phase (or of hydrate formed) for the system without SDS; slow gas enclathration rate for 500 ppm SDS; increase and then leveling off of the gas enclathration rate for higher SDS concentrations; and same amount of hydrate formed for SDS concentrations of 500 ppm and higher.

Fig. 5 shows $(dn_{g,r}/dt)_{max}$ as a function of SDS concentration for both types of experiment: (i) with 4000 ppm THF injected into the aqueous phase (open circles), and (ii) with 40,000 ppm THF present in the aqueous phase (full circles). The values of $(dn_{g,r}/dt)_{max}$ are also given in Table 1. Although the two curves exhibit the same general profile, significantly lower values (1.4–1.7 times lower) of $(dn_{g,r}/dt)_{max}$ were obtained for the experiments involving injection of 4000 ppm of THF. Moreover, the maximum value of $(dn_{g,r}/dt)_{max}$ seems to be reached at a lower SDS concentration (between 3000 and 4500 ppm as
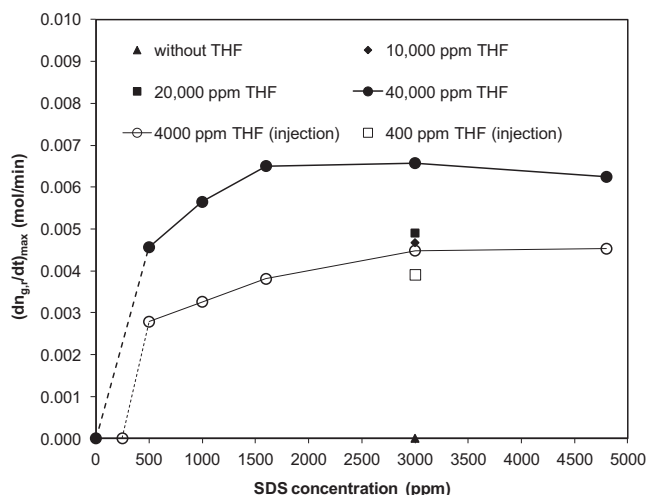

Fig. 5 – Maximum gas enclathration rate as a function of SDS concentration. Open symbols: THF is injected into the aqueous phase. Full symbols: THF is initially present in the aqueous phase (data from Ricaurte et al. (2013)).

opposed to between 1600 and 3000 ppm for the experiments with 40,000 ppm THF).

To obtain more insight into the relative influence of the THF and SDS concentrations on the measured kinetics of hydrate formation, we plotted in Fig. 5 the results of additional experiments carried out with 20,000, 10,000 and 0 ppm of THF present in a 3000 ppm SDS aqueous solution. $(dn_{g,r}/dt)_{max}$ is observed to significantly decrease with the THF concentration and to reach values close to that obtained after injecting 4000 ppm. Without THF, no hydrate formed, even after the system was left for longer than 24 h at T_{targ}.

These results clearly show that, at a given SDS concentration, the amount of THF used impacts the measured values of $(dn_{g,r}/dt)_{max}$, which therefore do not quantify exclusively the influence of the kinetic additive on the hydrate formation rate. They may nevertheless be assumed, because of the slight difference between the $(dn_{g,r}/dt)_{max}$ values at THF concentrations of 4000, 10,000 and 20,000 ppm, fairly representative of the intrinsic effect of 3000 ppm SDS on the crystallization kinetics of the CO_2–CH_4 hydrate at the pressure and temperature conditions of these experiments. The value of $(dn_{g,r}/dt)_{max}$ obtained for the experiment when 400 ppm of THF were injected into the aqueous phase (see the open square in Fig. 5), which differs by less than 13% from that at 4000 ppm THF, seems to confirm this point. It also indicates that the amount of THF must be reduced as much as possible to reduce its contribution to the measured hydrate formation rate and therefore enable the real influence of the kinetic additive to be determined.

Fig. 6 shows the variation in cell temperature during the experiment for different concentrations of THF and 3000 ppm SDS. For the systems with THF present in the aqueous phase at concentrations of 20,000 and 40,000 ppm, hydrate crystallization started before the cell temperature reached T_{targ}, while for 10,000 ppm THF, it occurred at T_{targ}. Although in the latter case, the hydrates crystallized at the target temperature, the time at which the crystallization began remained unpredictable due to the stochasticity of the phenomenon. In the experiments where 4000 ppm THF were injected, not only did crystallization occur at T_{targ}, but also its stochasticity was "canceled out", as the hydrate phase began to form a few seconds after the injection of THF.
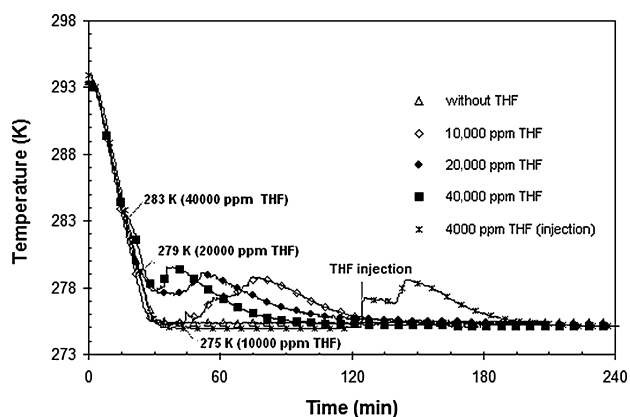
Fig. 6 – Cell temperature as a function of time for the systems with THF present in the aqueous phase at the concentrations of 0, 10,000, 20,000 and 40,000 ppm and for the system with 4000 ppm THF injected.

4. Conclusion

The experimental results presented in this work show that in situ injection of a small amount of THF into an aqueous phase in contact with a gas-hydrate-former phase at pressure and temperature conditions inside the hydrate metastable zone efficiently triggers hydrate crystallization. The most probable scenario is that the THF supersaturation produced at the injection point induces crystallization of a first hydrate rich in THF, which then triggers that of a second hydrate rich in the gas-hydrate-former phase.

This experimental method, which "cancels out" the stochasticity of hydrate crystallization, was used to evaluate the effect of the anionic surfactant SDS used at different concentrations on the formation kinetics of the CO_2–CH_4 hydrate at a temperature of 275 K.

Whether it is initially present or injected into the aqueous phase, THF was found to impact the formation rate of the CO_2–CH_4 hydrate: the higher the THF concentration (within the range of concentration tested), the higher the formation rate. Therefore, the intrinsic effect of the SDS on hydrate formation kinetics will be accurately evaluated only if the quantity of THF injected is very small. In the system studied here, 400 ppm of THF might be the appropriate concentration.

We believe that this experimental method for triggering the hydrate crystallization will be suitable for hydrate studies at low subcoolings, since it eliminates the long induction times generally observed at such conditions. In a future work, this method will be used for different subcoolings, and with various thermodynamic and kinetic hydrate promoters, such as cyclopentane and sodium dodecyl benzene sulfonate (SDBS).

References

Adeyemo, A., Kumar, R., Linga, P., Ripmeester, J., Englezos, P., 2010. Capture of carbon dioxide from flue or fuel gas mixtures by clathrate crystallization in a silica gel column. Int. J. Greenhouse Gas Control 4, 478–485.

Adisasmito, S., Frank, R.J., Sloan, E.D., 1991. Hydrates of carbon dioxide and methane mixtures. J. Chem. Eng. Data 36, 68–71.

Delahaye, A., Fournaison, L., Jerbi, S., Mayoufi, N., 2011. Rheological properties of CO_2 hydrate slurry flow in the presence of additives. Ind. Eng. Chem. Res. 50, 8344–8353.

Dicharry, C., Duchateau, C., Asbaï, H., Broseta, D., Torré, J.-P., 2013. Carbon dioxide gas hydrate crystallization in porous silica gel particles partially saturated sith a surfactant solution. Chem. Eng. Sci. 98, 88–97.

Duchateau, C., Peytavy, J.-L., Glénat, P., Pou, T.-E., Hidalgo, M., Dicharry, C., 2009. Laboratory evaluation of kinetic hydrate inhibitors: a procedure for enhancing the repeatability of test results. Energy Fuels 23, 962–966.

Duchateau, C., Glénat, P., Pou, T.-E., Hidalgo, M., Dicharry, C., 2010. Hydrate precursor test method for the laboratory evaluation of kinetic hydrate inhibitors. Energy Fuels 24, 616–623.

Gayet, P., Dicharry, C., Marion, G., Graciaa, A., Lachaise, J., Nesterov, A., 2005. Experimental determination of methane hydrate equilibrium curve up to 55 MPa by using a small amount of surfactant as hydrate promoter. Chem. Eng. Sci. 60 (21), 5751–5758.

Jerbi, S., Delahaye, A., Fournaison, L., Haberschill, P., 2010. Characterization of CO_2 hydrate formation and dissociation kinetics in a flow loop. Int. J. Refrig. 33 (8), 1625–1631.

Okutani, K., Kuwabara, Y., Mori, Y.H., 2008. Surfactant effects on hydrate formation in an unstirred gas/liquid system: an experimental study using methane and sodium alkyl sulfates. Chem. Eng. Sci. 63 (1), 183–194.

Park, K.-N., Hong, S.Y., Lee, J.W., Khang, K.C., Lee, Y.C., Ha, M.-G., Lee, J.D., 2011. A new apparatus for seawater desalination by gas hydrate process and removal characteristic of dissolved mineral (Na^+, Mg^{2+}, Ca^{2+}, K^+, B^{3+}). Desalination 274 (1–3), 91–96.

Rehder, G., Eckl, R., Elfgen, M., Falenty, A., Hamann, R., Kähler, N., Kuhs, W.F., Osterkamp, H., Windmeier, C., 2012. Methane hydrate pellet transport using the self-preservation effect: a techno-economic analysis. Energies 5 (7), 2499–2523.

Ricaurte, M., Dicharry, C., Broseta, D., Renaud, X., Torré, J.-P., 2013. CO_2 removal from a CO_2–CH_4 gas mixture by clathrate hydrate formation using THF and SDS as water soluble hydrate promoters. Ind. Eng. Chem. Res. 52 (2), 899–910.

Sefidroodi, H., Abrahamsen, E., Kelland, M.C., 2013. Investigation into the strength and source of the memory effect for cyclopentane hydrate. Chem. Eng. Sci. 87, 133–140.

Sloan, E.D., Koh, C.A., 2008. Clathrate Hydrates of Natural Gases, third ed. CRC Press, New York.

Tang, J., Zeng, D., Wang, C., Chen, Y., He, L., Cai, N., 2013. Study on the influence of SDS and THF on hydrate-based gas separation performance. Chem. Eng. Res. Des. 91 (9), 1777–1782.

Torré, J.-P., Dicharry, C., Ricaurte, M., Daniel-David, D., Broseta, D., 2011. CO_2 capture by hydrate formation in quiescent conditions: in search of efficient kinetic additives. Energy Proc. 4, 621–628.

Torré, J.-P., Ricaurte, M., Dicharry, C., Broseta, D., 2012. CO_2 enclathration in the presence of water-soluble hydrate promoters: hydrate phase equilibria and kinetics studies in quiescent conditions. Chem. Eng. Sci. 82, 1–13.

Veluswamy, H.P., Linga, P., 2013. Macroscopic kinetics of hydrate formation of mixed hydrates of hydrogen/tetrahydrofuran for hydrogen storage. Int. J. Hydrogen Energy 38, 4587–4596.

Wang, L., Zhang, X., Li, H., Shao, L., Zhang, D., Jiao, L., 2013. Theory research on desalination of brackish water using gas hydrate method. Adv. Mater. Res. 616–618, 1202–1207.

Zhang, J.S., Lo, C., Somasundaran, P., Lu, S., Couzis, A., Lee, J.W., 2008. Adsorption of sodium dodecyl sulfate at THF hydrate/liquid interface. J. Phys. Chem. C 112 (32), 12381–12385.

Zhong, Y., Rogers, R.E., 2000. Surfactant effects on gas hydrate formation. Chem. Eng. Sci. 55 (19), 4175–4187.